Design of DC Permanent Magnet Disc Motor and Improving its EMC

Irena KOVÁČOVÁ, Ján KAŇUCH, Dobroslav KOVÁČ

Technical University of Košice, Slovakia

***Summary*: The paper deals with construction design of DC permanent magnet disc motor by classical calculation method and its verifying by computer finite element simulation method. The paper deals also with the computer analysis of the electromagnetic compatibility (EMC) problems focused to the area of electrical machines, which can also disclose the startling facts concerning. A problem of interference between electric motor and surroundings space caused by electromagnetic field radiation is discussed too.**

Keywords: *electromagnetic compatibility, disc motor, electromagnetic field radiation*

1. INTRODUCTION

The most frequently manner of electric energy utilization in industry is their conversion to mechanical power. For the drives, which needs to have a great dynamics, is necessary to choice the motor from the group of disc motors. Motors we can divide into two groups according the feeding voltage properties. First is created by AC motors and the second by DC motors. From the EMC problem point of view the DC motors seems to be better than AC motors thanks to their DC load current and static magnetic field with the given orientation. In due to its weight and dimensions reduction they can be utilized in many modern automated electrical drives. The facts as simple control process and possibility of its utilizing in battery powered autonomous systems are arguments for DC permanent magnet (PM) disc motor selection. By the classic design of DC permanent magnet (PM) motor we will show that no recognizing of EMC knowledge can leads to the unfavorable EMC parameters of these motors despite of the existence of strong static magnetic field created by their permanent magnets.

Importance of electromagnetic compatibility (EMC) of all electrical products is rapidly increasing during the last decade. The quality of life environment is increasingly polluted with electromagnetic energy. The interference output into the surroundings is doubled every three years, and covers a large frequency range.

The possibility of equipment disturbances and mistakes becomes more serious as consequence of the electronic circuit complexity growth. According the new technical legislation and also in due to economic consequences the EMC concept of all products must be strictly observed. It must start with the equipment performance specifications and finish with equipment installation procedures.

2. CLASSIC METHOD OF PM MOTOR DESIGN

In following the detail electromagnetic design of disc motor with separately driving poles made from permanent magnets will be done.

The design basis consists in required nominal motor parameters, which are:

— Nominal motor power: $P_N = 300$W
— Engine speed: $n_N = 3000$ turns/min.
— Nominal feeding voltage: $U_N = 70$ V

2.1. Calculation of the Main Rotor Dimensions

The main rotor dimensions (average rotor diameter D_S and effective length of winding l_e) is possible to calculate by value of internal electric motor power P_i given for nominal turns $n_N = 3000$ turns/min. and nominal motor power $P_N = 300$W. In the case of DC motor power values up to 1 kW and typical efficiency $\eta = 0{,}75$, the internal power P_i can be acquired as average value calculated from nominal output and input powers.

$$P_i = \frac{1+\eta}{2\cdot\eta}\cdot P_N = \frac{1+0{,}75}{2\cdot 0{,}75}\cdot 300 = 350\,\text{W} \qquad (1)$$

In dependency on ratio P_N / n_N (in our case 300/3000 = 0,1) the designed rotor diameter can have value within the range 0,12 m up to 0,14 m.

With respect to the expected rotor diameter and geometrical structure of disc motor magnetic circuit it is also possible to pre-set the number of motor poles as value $2p = 10$.

Then for practical rotor diameter calculation is possible to use equation:

$$D = b_1 + b_2 \cdot \sqrt[3]{\frac{p \cdot P_i}{\lambda \cdot n_1}} \qquad (2)$$

where:

$b_1 = 0{,}075$ and $b_2 = 0{,}0128$ (for $D < 1$ m),
$2p$ is number of motor poles,
λ is ratio of effective winding length and pole spacing ($\lambda = l_e/\tau_p$),
n_1 is motor speed given as turns per second ($n_1 = n_N / 60 = 3000/60 = 50$ tr./s).

Rotor diameter is possible to state under condition that the ratio λ of effective winding length and pole spacing will stated in advance.

$$\lambda = \frac{l_e}{\tau_p} \tag{3}$$

This ratio is obviously within the range from 0,5 up to 2. In our case will be choices $\lambda = 0{,}9$. Rotor diameter is possible to calculate now by equation (2).

$$D = 0{,}075 + 0{,}0128 \cdot \sqrt[3]{\frac{5 \cdot 350}{0{,}9 \cdot 50}} = 0{,}118\,\text{m} \tag{4}$$

For obtained rotor diameter $D = 0{,}118$ m is pole spacing τ_p given by following equation.

$$\tau_p = \frac{\pi \cdot D}{2p} = \frac{\pi \cdot 0{,}118}{10} = 0{,}03707\,\text{m} \tag{5}$$

Effective winding length can be calculated now by equation (3).

$$l_e = \lambda \cdot \tau_p = 0{,}9 \cdot 0{,}03707 = 0{,}03364 \cong 0{,}034\,\text{m} \tag{6}$$

With respect on motor construction solution it is chosen minimal rotor diameter $D_{\min} = 0{,}089$ m. As consequence of calculated effective winding length $l_e = 0{,}034$ m the maximal rotor diameter is:

$$D_{max} = D_{min} + 2 \cdot l_e = 0{,}089 + 2 \cdot 0{,}034 = 0{,}157\,\text{m} \tag{7}$$

Average rotor diameter is possible to state as:

$$D_s = \frac{D_{min} + D_{max}}{2} = \frac{0{,}089 + 0{,}157}{2} = 0{,}123\,\text{m} \tag{8}$$

Based on calculated value of average rotor diameter the real pole spacing τ_{ps} can be recalculated, too.

$$\tau_{ps} = \frac{\pi \cdot D_s}{2p} = \frac{\pi \cdot 0{,}123}{10} = 0{,}03864\,\text{m} \tag{9}$$

2.2. Rotor Winding Design

Rotor current is possible approximately to state by relation:

$$I_N = \frac{P_N}{U_N \cdot \eta} \cdot \left(1 - \frac{1-\eta}{7 \cdot \eta}\right) = \frac{300}{70 \cdot 0{,}75} \cdot \left(1 - \frac{1-0{,}75}{7 \cdot 0{,}75}\right) = 5{,}986\,\text{A} \tag{10}$$

Number of rotor conductors N_v we can calculate as:

$$N_v = \frac{\pi \cdot D_s \cdot H}{I} \cdot 2a \tag{11}$$

where:

D_s is average rotor diameter of disk motor,
H is rotor magnetic intensity [A/m],
$2a$ is number of parallel-connected rotor branches.

If we consider the influence of rotor diameter on its magnetic intensity H and also influence of magnetic intensity H on commutation, so for electric motors with small rotor diameters the value of magnetic intensity should be $H < 5.10^3$ A/m.

Respecting the disc rotor construction solution (multilayer winding) and its dimensions the rotor magnetic intensity is chosen as $H = 2{,}74.10^3$ A/m. A wave winding is also designed with the parameter $2a = 6$. After such assignation of required values it is possible to calculate the number of winding conductors by equation (11),

$$N_v = \frac{\pi \cdot 0{,}123 \cdot 2{,}74.10^3}{5{,}986} \cdot 3 = 1061{,}186 \tag{12}$$

Obtained value of winding conductors is possible to round as $N_v = 1062$ and according equation (11) is necessary to state real amount of rotor magnetic intensity.

$$H = \frac{N_v \cdot I}{\pi \cdot D_s \cdot 2a} = \frac{1062 \cdot 5{,}986}{\pi \cdot 0{,}123 \cdot 6} = 2{,}742.10^3\ \text{A/m} \tag{13}$$

Motor induced voltage is possible approximately to state according expression:

$$U_i = U_N - 0{,}5 \cdot (1-\eta) \cdot U_N = 70 - 0{,}5 \cdot (1 - 0{,}75) \cdot 70 = 61{,}25\,\text{V} \tag{14}$$

Magnetic flux can be determine by motor's induced voltage and next equation:

$$\phi = \frac{U_i}{N_v \cdot \frac{p}{a} \cdot n_1} = \frac{61{,}25}{1062 \cdot \frac{5}{3} \cdot 50} = 6{,}92.10^{-4}\ \text{Wb} \tag{15}$$

In the case of disc rotor the commutator brushes are sealing directly on rotor winding, which at the same time serves as commutator segment. The number of commutator segments K_1 is equal to the number of conductors N_{v1} on one disc side, where are touching-down the commutator brushes. If v is number of disc rotor layers and it will be chosen as $v = 6$, so then the number of conductors N_{v1} in one layer can be calculated as:

$$N_{v1} = \frac{N_V}{v} = \frac{1062}{6} = 177 \tag{16}$$

Number of commutator segments is:

$$K_1 = N_{v1} = 177 \tag{17}$$

Although the designed disc rotor have no classic grooves, even though the fictive number of groves is equal to the number of commutator segments.

$$Q = K_1 = 177 \tag{18}$$

The number of groves falling on one motor pole one can reach as ratio of fictive number of groves and the number of poles.

$$Q_p = \frac{Q}{2p} = \frac{177}{10} = 17{,}7 \tag{19}$$

Next relation expresses the pole spacing τ_{pd}, which is equal to the number of groves falling on one motor pole.

$$\tau_{pd} = Q_p = 17{,}7 \tag{20}$$

Back grove step characterized by inequality $y_{d1} > t_{pd}$ is selected as $y_{d1} = 18$. Grove winding step is established on the basis of equation:

$$y_d = \frac{Q+a}{p} = \frac{177+3}{5} = 36 \tag{21}$$

Rotor grove spacing τ_d is given as:

$$\tau_d = \frac{\pi \cdot D_s}{Q} = \frac{\pi \cdot 0{,}123}{177} = 0{,}00283\,\text{m} \tag{22}$$

Number of conductors in grove is the same as number of disc rotor layers. We can state it by relation:

$$V_d = \frac{H \cdot \tau_d \cdot 2a}{I} = \frac{2{,}742.10^3 \cdot 0{,}00283 \cdot 6}{5{,}986} = 6 \tag{23}$$

Number of winding solenoids will be:

$$N_c = \frac{N_V}{2} = \frac{1062}{2} = 531 \tag{24}$$

As result of the rotor disc construction fact that one solenoid of the wave winding is situated in two mutual isolated rotor layers (front solenoid side in first and back solenoid side in second), so commutator winding step y_k will be calculated by equation:

$$y_k = \frac{v}{2} \cdot y_d = \frac{6}{2} \cdot 36 = 108 \tag{25}$$

Cross section area of rotor winding conductors can be found by total motor current value, by number of one feeding pole brushes and by value of maximal allowable current density.

$$S_v = \frac{I}{N_u \cdot \sigma} = \frac{5{,}986}{2 \cdot 6} = 0{,}4989\,\text{mm}^2 \tag{26}$$

where:
N_u is number of one feeding pole brushes. In due to carbon dimension reduction the number is chosen as $N_u = 2$.
$\sigma = 6$ A/mm^2 is maximal allowable current density.

If disc rotor winding will be made from conductor with rectangle cross-section area $S_v = b_v \,.\, h_v$ and its high will be chosen as $h_v = 0{,}4$ mm, then its width b_v will be:

$$b_v = \frac{S_v}{h_v} = \frac{0{,}4989}{0{,}4} = 1{,}24725\,\text{mm} \tag{27}$$

Figure 1 shows a part of designed disc rotor winding (one layer – front solenoid sides) with presentation of some calculated parameters.

Figure 2 displays schematic cut of six layers disc rotor with the depiction of currents direction in individual layers. The technique of individual layers (pointed weld) mutual interconnection, so that wave winding will be created, is displayed too.

Rotor thickness h_r can be stated on the basis of cooper winding layer thickness h_v and isolated layer thickness h_i (polyamide prepreg).

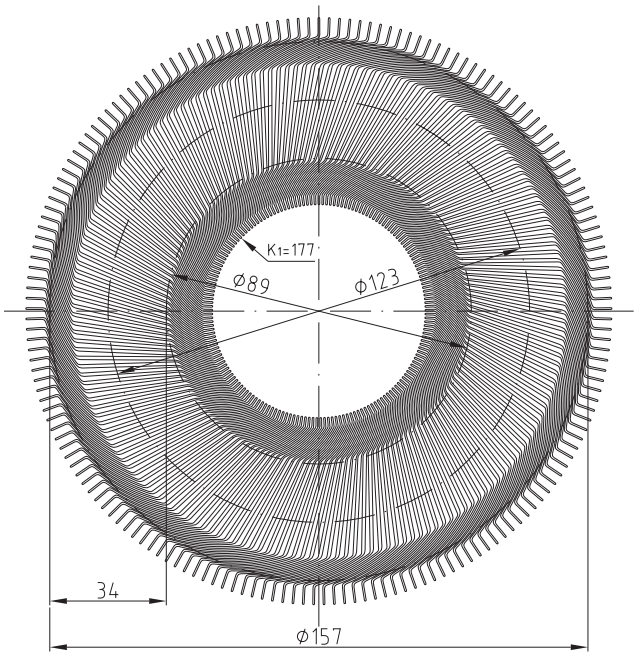

Fig. 1. One layer of designed disc rotor winding

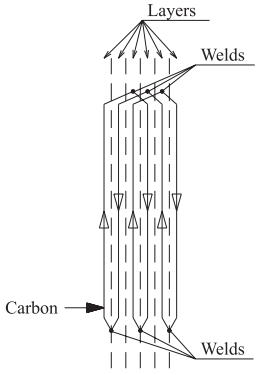

Fig. 2. Schematic cut of six layers disc rotor

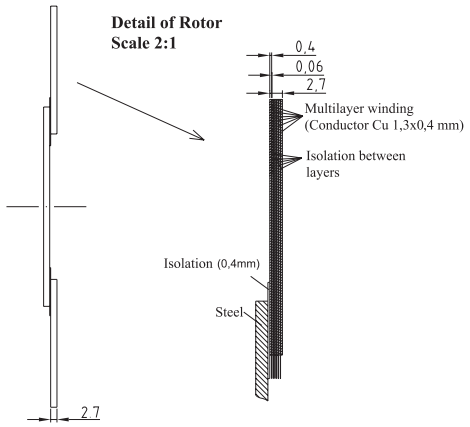

Fig. 3. Partial cut of the designed rotor disc

$$h_r = V_d .h_v + (V_d - 1).h_i = 6.0,4 + (6-1).0,06 = 2,7\,\text{mm} \quad (28)$$

Figure 3 shows rotor details, it means, partial cut of the designed rotor disc.

2.3. Pole Extension Design

The shapes and dimensions of pole extension are obviously chosen so that its inside magnetic saturation may not come into existence and leakage magnetic flux must be minimal. The pole extension length is obviously the same or a bit smaller than rotor length in classic DC machines. In due to fact that in our case the rotor has the disc shape, so the length of pole extension h_p will be chosen as the same as effective rotor length l_e, calculated from equation (6)

$$h_p = l_e = 0,034\,\text{m} \quad (29)$$

Pole extension width s_p depends on pole spacing τ_p and chosen pole covering λ_p. For pole spacing calculated according (9) we can choice pole covering $\lambda_p = 0,65$. Pole extension width is then possible to obtain by equation:

$$s_p = 1,05 \cdot \lambda_p \cdot \tau_p = 1,05 \cdot 0,65 \cdot 0,03864 = \\ = 0,026373 \cong 0,0264\,\text{m} \quad (30)$$

Respecting the requirement of leakage magnetic flux minimalization and disc rotor winding shape, the pole extension, which fashion is shown in Figure 4, was designed.

Figure 5 displays lateral view on designed pole form. Final pole dimensions l_{pn} and l_m will be calculated in chapter dealing with the motor magnetic circuit projection.

Figure 6 shows motor pole arrangement at stator frame.

For wave winding creation the layer with back solenoid sides must be as mirror picture of the layer with front solenoid sides, but also designed grove step y_d, depending on the number of motor poles, must be respected. Wave winding, the part of which is shown in Figure 7, will originate by front and back solenoid sides interconnecting.

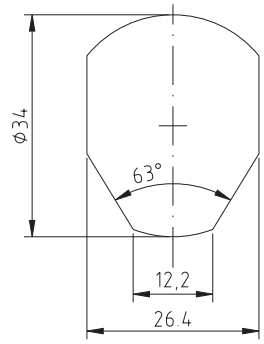

Fig. 4. Designed pole extension fashion

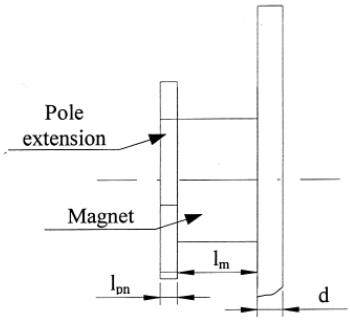

Fig. 5. Lateral view on designed pole

2.4. Carbon Dimension Design and Disc Motor Construction Design

Spacing between lamellas for chosen commutator diameter $D_k = 0,077$ m is:

$$\tau_1 = \frac{\pi \cdot D_k}{K_1} = \frac{\pi \cdot 0,077}{177} = 1,3667.10^{-3}\,\text{m} \quad (31)$$

Typical value of carbon width b_u is within the range (2 up to 4).σ_1, it means (2,73 up to 5,47).10^{-3} m. Let the carbon current density will be σ_u = 5 A/cm^2, then we can state the total carbon cross-section area as:

$$S_{uc} = \frac{I}{N_u \cdot \sigma_u} = \frac{5,986}{2 \cdot 5} = 0,5986\,\text{cm}^2 \quad (32)$$

If the number of one pole brushes are selected as $N_u = 2$, so also two carbons is necessary to have. It means that also total calculated cross-section area must be divided on two areas $S_u = S_{uc}/2$. Carbon width is chosen as $b_u = 4$ mm. By next relation we can calculate its high.

$$h_u = \frac{S_u}{b_u} = \frac{0,2993.10^2}{4} = 7,48\,\text{mm} \quad (33)$$

After rounding the carbon have dimensions b_u x v_u = 4 x 8 mm. Lamellas distance is:

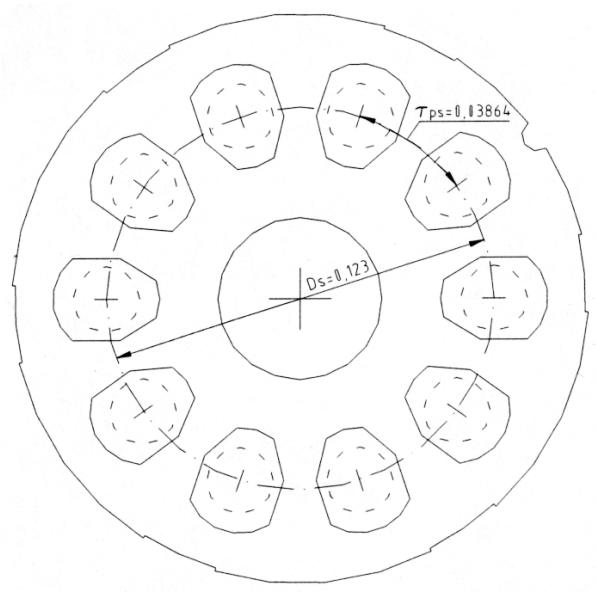

Fig. 6. Motor pole arrangement at stator frame

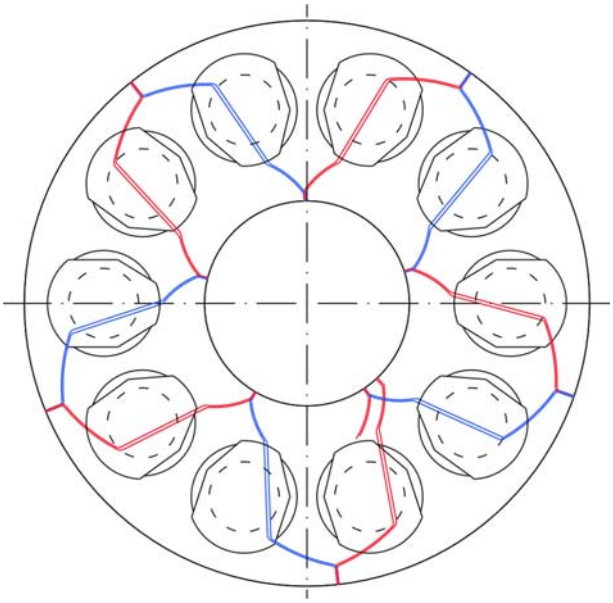

Fig. 7. Part of disc rotor wave winding

$$h_l = \frac{\pi \cdot D_k}{K} - b_v = \frac{\pi \cdot 0{,}077}{177} - 0{,}00124725 = \\ = 0{,}119432.10^{-3}\,\mathrm{m} \tag{34}$$

The number of lamellas (conductors) under carbon is possible to state as:

$$p_{lu} = \frac{b_u}{\frac{\pi \cdot D_k}{K} - h_l} = \frac{0{,}004}{\frac{\pi \cdot 0{,}077}{177} - 0{,}119432.10^{-3}} = 3{,}2 \cong 4 \tag{35}$$

From obtained result one can see, that carbon, with chosen dimensions, covers 4 commutator lamellas (it means that it is supplying 4 solenoids). The situation is shown in Figure 8, where is displayed rotor detail with depicted carbon holder.

Figure 9 shows part of disc rotor winding, which is flowed by current, and motor poles.

Figure 10 is representative disc motor construction solution together with motor shaft. A part of multilayer disc rotor winding is displayed where the individual layers are pasted together via isolation material (for example polyimide prepreg), which has very good mechanical properties after hardened. Together with the winding it creates solid mechanical disc with required dimensions.

Soldered interconnection of individual layers is created by the demand of wave winding construction with the extended step. Regard to the space problem the individual layers must be mutually shifted. Figure 11 shows in detail the partial axial cut of disc rotor at the position between two poles.

Rectangles are representing winding conductors in layers, which are mutually isolated and glued so, that creates compact disc. Undercurrent conductors are marked by black color.

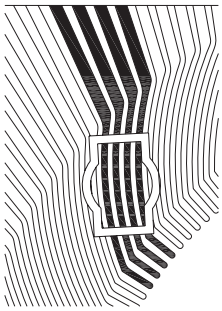

Fig. 8. Detail part of rotor with displaying of carbon holder

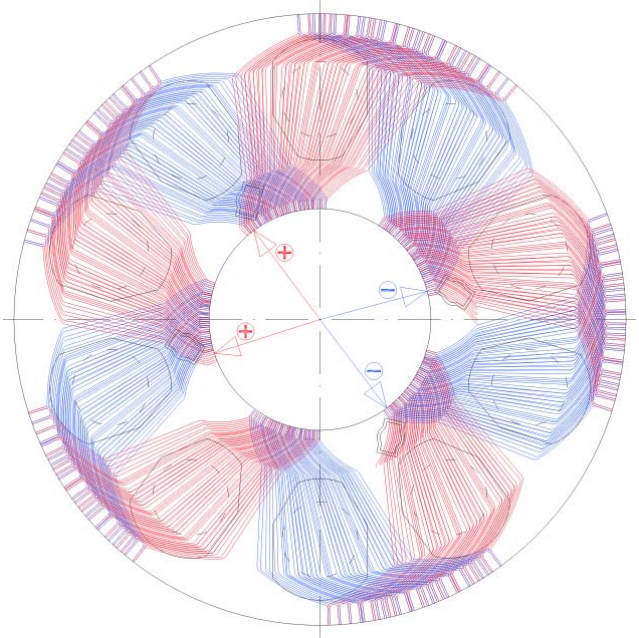

Fig. 9. Part of disc rotor winding, which is flowed by current

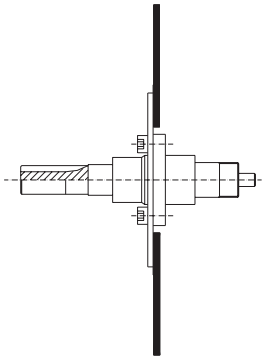

Fig. 10. Construction solution of disc rotor

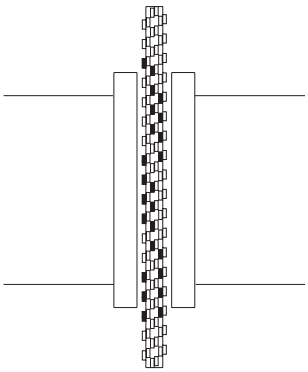

Fig. 11. Partial axial cut via disc rotor

2.5. Design of Magnetic Circuit and Motor Construction

For total magnetic circuit design and its calculation is necessary, beside area size S_v and length size l_v of air gap, to project also area size S_m and length of permanent magnets, pole extension thickness l_{pn}, thickness d and also minimal R_{min} and maximal R_{max} radiuses of stator frame.

During magnetic circuit air gap dimension l_v stating the fact, that the designed rotor thickness h_r is 2,7 mm and that the bearings, in which the rotor will be mounted, can caused its vibration between pole extensions only within the range ± 0,5 mm, must be respected. If the additional safety distance with the size ± 0,1 mm will be considered, so the final design of air gap dimension l_v can be done.

$$l_v = 0{,}1 + 0{,}5 + h_r + 0{,}5 + 0{,}1 = \\ = 0{,}1 + 0{,}5 + 2{,}7 + 0{,}5 + 0{,}1 = 3{,}9\,\text{mm} \quad (36)$$

If none leakage magnetic flux in designed magnetic circuit air gap will be reasoned, so the air gap area size S_v can be the same as pole extension area size.

$$S_v = S_{pn} = 0{,}0007443424\,\text{m}^2 \quad (37)$$

The permanent magnet cross-section area size S_m is possible to state by pole extension dimensions and Figure 12 so, that inside the pole extension will be pictured circle with the radius, which will be smaller than the smallest distance from centre to the edge of designed pole extension. The smallest distance to the pole extension edge is 13,2 mm. In due to magnetic field homogenity it is the best choice of permanent magnet radius 10,6 mm. The permanent magnet cross-section area will be then:

$$S_m = \pi . R_m^2 = \pi . (0{,}0106)^2 = 0{,}000352989\,\text{m}^2 \quad (38)$$

Pole extension thickness l_{pn} is possible to receive from reason, that it should be the same as the difference between one half of pole extension width and permanent magnet radius.

$$l_{pn} = \frac{s_p}{2} - R_m = 13{,}2 - 10{,}6 = 2{,}6\,\text{mm} \quad (39)$$

Minimal stator frame radius R_{min} is first of all given by outer diameter of used bearing. In our case the bearing is chosen with outer diameter $\Phi = 40$ mm. Minimal stator frame radius we can choice as $R_{min} = 20$ mm.

Maximal stator frame radius R_{max} is given by designed disc rotor radius, weld sizes of wave winding at outer rotor edge and by certain safety distance between rotor and stator. On the basis of above-mentioned the maximal stator frame radius was stated as $R_{max} = 91{,}5$ mm.

Stator thickness d is possible to calculate on the basis of required magnetic flux value, stator cross-section area S_z and stator maximal required magnetic saturation B_{dov} related to the chosen construction material. For stator and pole

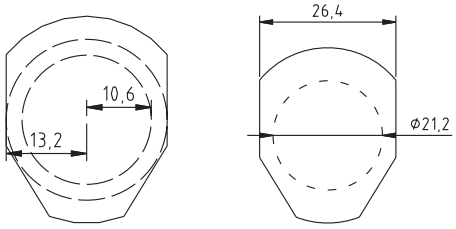

Fig. 12. Design of permanent magnet cross-section area

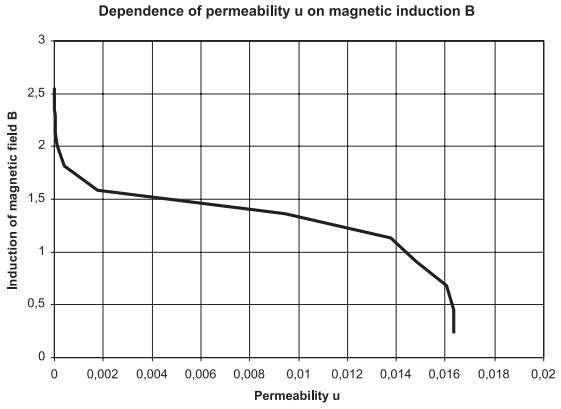

Fig. 13. Pure steel dependence of permeability m on magnetic induction *B*

Table 1

B [T]	H [A.m^{-1}]	μ [H.m^{-1}]
0,227065	13,8984	0,01633749
0,45413	27,7967	0,01633755
0,681195	42,3974	0,01606691
0,90826	61,4157	0,01478873
1,13533	82,3824	0,01378122
1,36239	144,669	0,00941729
1,58935	897,76	0,00177035
1,81236	4581,74	0,00039556
2,01004	17736,2	0,00011333
2,19999	68321,8	3,22E-05
2,25479	95685,5	2,3565E-05
2,29993	123355	1,8645E-05
2,34251	151083	1,5505E-05
2,37876	178954	1,3293E-05
2,41501	206825	1,1677E-05
2,45126	234696	1,0444E-05
2,4875	262568	9,4737E-06
2,52375	290439	8,6894E-06
2,56	318310	8,0425E-06

extension construction was selected pure steel material with magnetizing characteristic described in table Table 1 and pictured in Figure 13.

Based on this characteristic it is possible to state the maximal allowable magnetic induction as $B_{dov} = 2{,}54$ T. For stator frame thickness d calculation is then valid relation:

$$d = \frac{\phi}{B_{dov}.(R_{max} - R_{min})} = \frac{6{,}92.10^{-4}}{2{,}54.(0{,}0915 - 0{,}02)} = 0{,}00381\,\mathrm{m} \tag{40}$$

The last magnetic circuit parameter, permanent magnet length l_m, could be stated only on the basis of calculation. For this purpose must be taken into account also the equivalent scheme of ten poles DC PM disc motor magnetic circuit, which is pictured in Figure 14.

By the scheme in Figure 14 the basic equation, which will be utilize for magnetic circuit calculation, can be derived.

$$4 \cdot U_m = \left(4 \cdot R_{mpn} + 4 \cdot R_m + 2 \cdot R_{mv} + R_{mž}\right) \cdot \Phi \tag{41}$$

where:

U_m is magnetic voltage,
R_{mp} is magnetic resistance of pure steel pole extension part,
R_{mag} is permanent magnet magnetic resistance,
R_{mv} is air gap magnetic resistance,
$R_{mž}$ is lateral cover magnetic resistance, but only within the distance between individual motor poles.

Stating of individual motor part magnetic resistances was done on the basis of well-known fundamental relation:

$$R_m = \frac{1}{\mu} \cdot \frac{l}{S} \tag{42}$$

For construction of motor poles, which are generating the exciting magnetic flux, the permanent magnets from SmCo 27 MGOe were used. Their coercivity value is H_c =

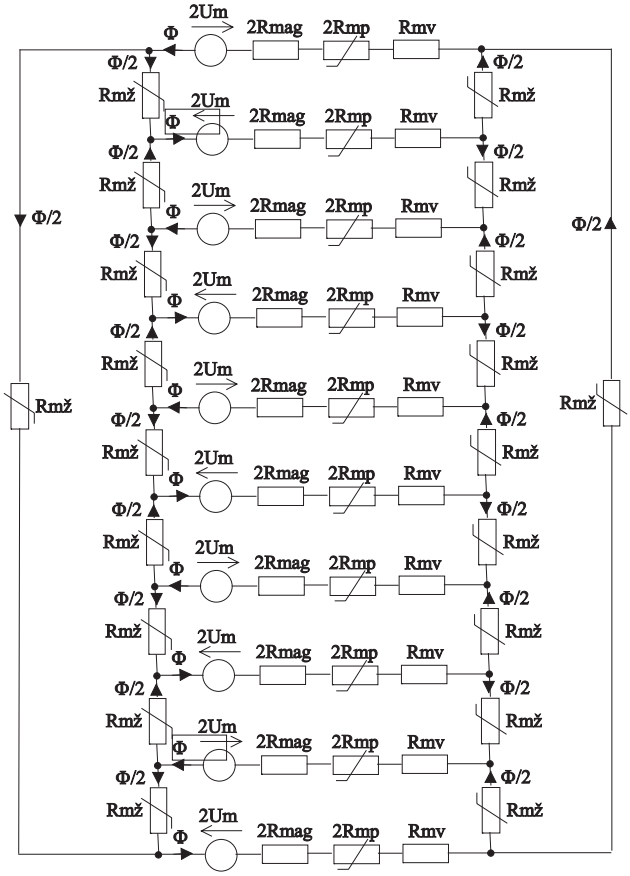

Fig. 14. Equivalent scheme of ten poles DC PM disc motor magnetic circuit

774000 A.m^{-1} and relative permeability is $m_{rm} = 3.8$. Asked permanent magnet length l_m could be received by adapted equation (41).

$$4 \cdot H_c . l_m = \tag{43}$$

$$= \left(4 \cdot \frac{l_m}{\mu_m . S_m} + 4 \cdot \frac{l_{pn}}{\mu_{pn} . S_{pn}} + 2 \cdot \frac{l_v}{\mu_0 . S_v} + \frac{\tau_{ps}}{d(R_{max} - R_{min})}\right) \cdot \Phi$$

$$l_m = \frac{\left(4 \cdot \frac{l_{pn}}{\mu_{pn} . S_{pn}} + 2 \cdot \frac{l_v}{\mu_0 . S_v} + \frac{\tau_{ps}}{\mu . d(R_{max} - R_{min})}\right) \Phi}{(4 \cdot H_c - \frac{4.\Phi}{\mu_m . S_m})} = \tag{44}$$

$$= \frac{\left(4 \cdot \frac{0{,}0026}{1{,}41.10^{-2}.0{,}0007443424} + 2 \cdot \frac{0{,}0039}{4\pi.10^{-7}.0{,}0007443424} + \frac{0{,}03864}{8{,}07.10^{-6}.0{,}00381(0{,}0915 - 0{,}02)}\right) \cdot 6{,}92.10^{-4}}{(4 \cdot 774000 - \frac{4.6{,}92.10^{-4}}{4\pi.10^{-7}.3{,}8.0{,}000352989})} =$$

$$= 0{,}01233561\ m \doteq 0{,}0124\ m$$

General overview of individual designed and calculated parameters of magnetic circuit is listed in table Table 2.

After main motor parameters calculation it is possible to start the design of its construction solution. Figure 15 shows the arrangement of motor poles at right stator side and also is

Table 2

		Parts of motor magnetic circuit			
		Permanent magnet	Pole extension	Stator	Air gap
S	**[m^2]**	0,000352989	0,0007443424	0,000272415	0,0007443424
l	**[m]**	0,0124	0,0026	0,03864	0,0039
μ	**[$H.m^{-1}$]**	$4{,}775.10^{-6}$	$1{,}41.10^{-2}$	$8{,}07.10^{-6}$	$1{,}2566.10^{-6}$
B	**[T]**	1,960401032	0,929680174	2,54024191	0,929680174
R_m	**[H^{-1}]**	7356769,301	247,731	17576506,76	4169606,073

pictured the location of two pairs of motor brushes. Figure 16 displays the motor in decomposed state.

Figure 17 displays built-up plan of PM disc motor and in figures 18 up to 20 are pictured practical realization samples of individual motor parts.

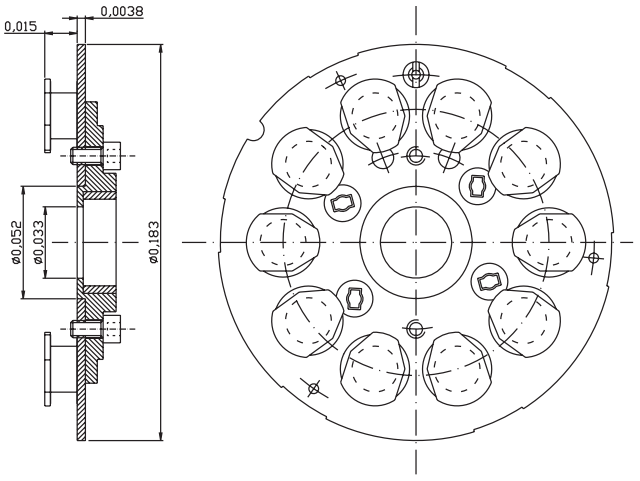

Fig. 15. Cut via motor and internal view on right

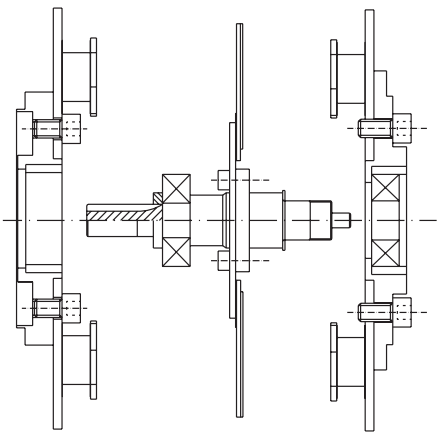

Fig. 16. Motor in decomposed state stator side

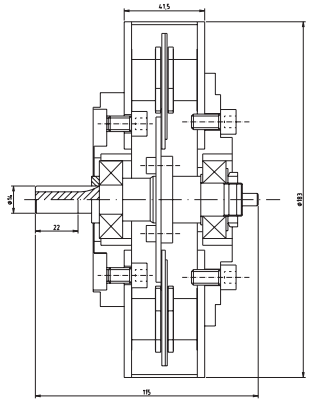

Fig. 17. Drawing of DC PM disc motor built-up plan

Fig. 18. Rotor

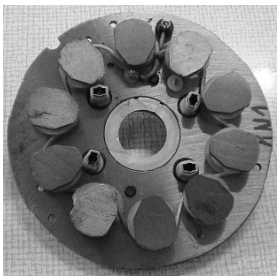

Fig. 19. Right side of stator

Fig. 20. Left side of stator

3. VERIFICATION OF MOTOR MAGNETIC CIRCUIT DESIGN BY COMPUTER NUMERICAL SIMULATION

Design correctness of DC PM disc motor could be attested by utilizing of numerical computer simulation methods for its magnetic field finding. Figure 21 shows graphical and numerical results of such computer analysis where finite element method was used. In due more simplification it will be supposed that rounded ten poles stator of DC PM disc motor is expanded into the plane.

Relative error d of the theoretical model is possible to state by magnetic fields comparing, which are obtained by classical and numerical solutions in individual places A, B, C, and D of motor magnetic circuit. Maximal of these errors is very probably representing also the deviation error of total motor design. Relative error in point A is $\delta_A = 2{,}519\%$, in point B is $\delta_B = 0{,}357\%$, in point C is $\delta_C = -14{,}208\%$ and in point D is $\delta_D = 0{,}355\%$. From above mentioned results it is clear that the biggest inaccuracy can come into existence during pole extension designing, because in this position the error between both methods is the biggest. This difference is caused by this fact that within small pole extension dimensions exists great magnetic field gradient and also that magnetic field is closed not only by main magnetic circuit, but by leakage ways, too.

4. EMC OF DC PM DISC MOTOR

From results obtained by computer numerical simulation and pictured in Figure 21 is evident, that motor magnetic field is not closed only inside of the motor, but it is also reaching its near space. Such a way it is clear, that in the case of EMC investigation of power electrical engineering systems the motor load must be taken into account, too. Results obtained by such analysis will be valid not only for DC PM disc motors, but also for the rest DC and AC electrical machines.

4.1. Simulation and Measuring of Motor EMC

Let we try to state the motor EMC. For this purpose the numerical computer simulation method of magnetic field will be utilized. Point A represents place where the leakage field between left and right motor poles is closed. The field is almost homogenous in this place. Position of point B is chosen so, that it is located on the one edge of permanent magnet motor poles. Motor magnetic field is periodically located around the motor perimeter. Number of periods is corresponding to the number of motor pole pairs. From the EMC investigation point of view will be very interested to find beside magnetic field absolute value also the real time magnetic field change, which is caused by the change of its working conditions. The change of magnetic field is inducing ineligible voltages in electrical loops of an around electric circuits. Magnetic field change is created besides the regulation moments also in steady state working condition, if the motor is supplied from a power semiconductor converter. This case is very frequently in modern electrical drive systems. DC motor speed is then proportional to the average value of motor supply voltage, which is the same as average value of converter's output voltage. From DC electrical machine theory is known that the motor moment is directly proportional to its current. Equivalent electrical scheme of DC motor is represented by serial connection of resistor, inductor and induced voltage source. The shape of output current from impulse voltage converter will be not constant. Also during the steady state motor working conditions the motor has periodical and dynamical moment undulating corresponding to its current undulating. Measured curves of switching IGBT transistor voltage u_{CE} and the load current i_Z are shown in Figure 22. The IGBT transistor is connected as main part of

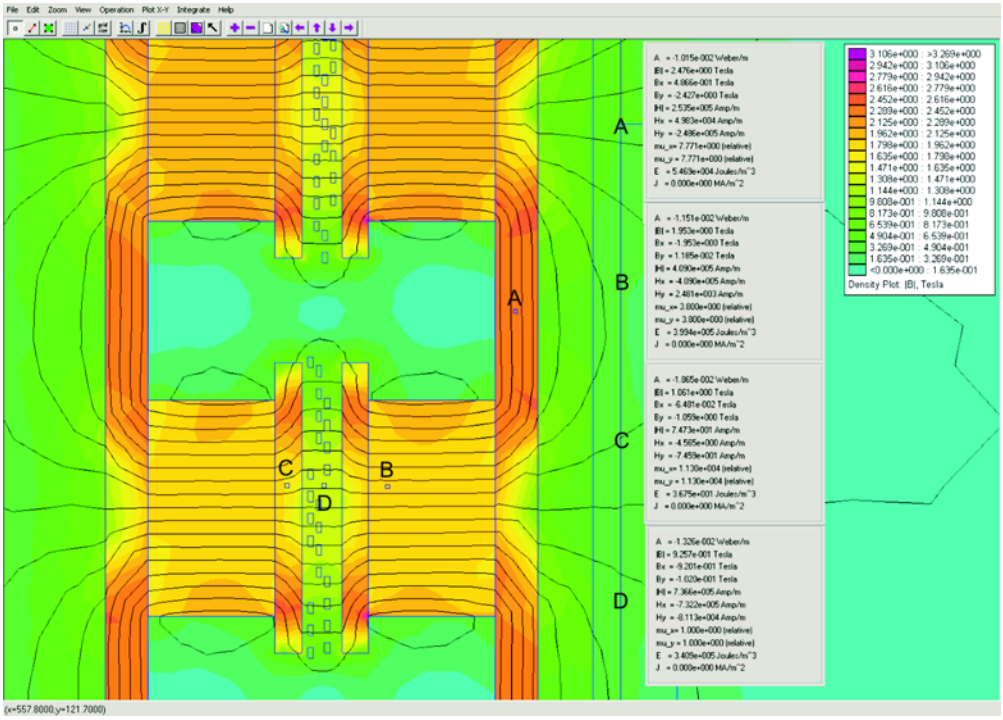

Fig. 21. Motor magnetic field arrangement obtained by computer numerical simulation

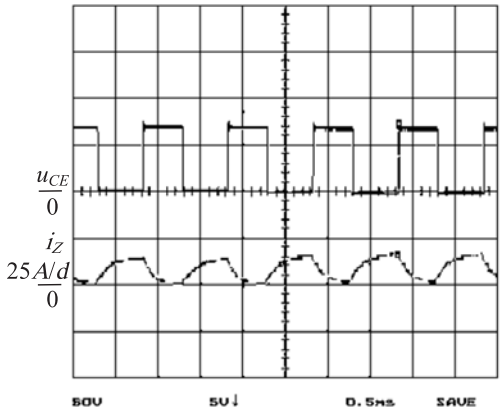

Fig. 22. Measured curves of IGBT transistor voltage u_{CE} and motor current i_Z

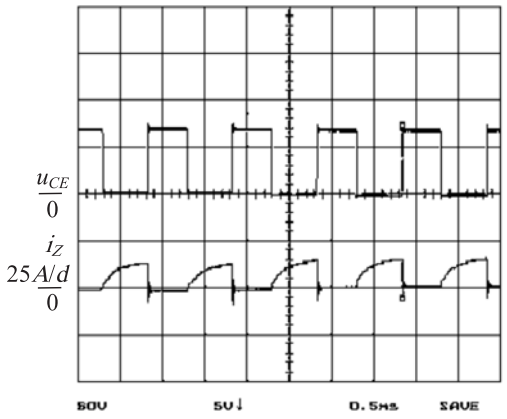

Fig. 23. Measured curves of IGBT transistor voltage u_{CE} and current i_C

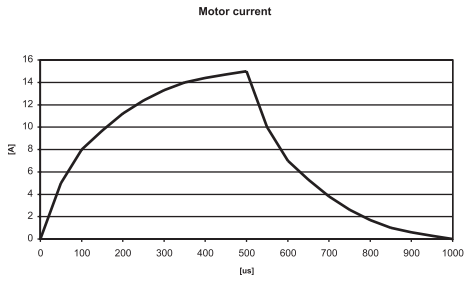

Fig. 24. Approximated motor current i_Z curve obtained by Excel program

one quadrant DC voltage impulse power semiconductor converter. The load is represented by DC PM disc motor. Figure 23 displays curves of insulated gate bipolar transistor (IGBT) voltage u_{CE} and current i_C.

Time dependence of measured motor current i_Z is possible to approximate by Excel program. Resulting curve is pictured in Figure 24.

Table form of load current values i_Z for given time moments is listed in table Table 3.

Let the magnetic field numerical analysis will be done for two extreme values of load current i_Z in next step. For I = 0 A and I = 15 A. If the difference of obtained magnetic field values, corresponding to above mentioned currents, will be multiplied by the loop area size S = 0,1 x 0,05 m of the other electrical circuit and divided by time difference, in which the individual current was sampled, so then we can obtain the imagination about the interference of induced voltage amount.

Resulting magnetic field values are shown in Figure 25 for the current i_Z value at the moment of switching period start and in the places of both investigated points.

Results for the same geometric and material conditions are shown in Figure 26, but at the moment of maximal load current i_Z magnitude. It means at middle of switching period when current has value I = 15A.

By above-mentioned method and by simulation was obtained values of magnetic field inductions B and induced voltages u_i for all current i_Z values listed in table 3. Results are presented in table 4.

Graphical interpretation of magnetic induction B in dependence on time is pictured in figures 27 and 28. Induced voltage u_i curve is shown in Figures 29 and 30.

On the basis of facts presented in previous it is able to find out that the biggest magnitude of induced voltage is during the time of the biggest slope of motor current growth or fall in position A. It is coming up at the moments of growing and falling edges of feeding voltage impulse given from power semiconductor converter. The induced voltage peaks then reaches values up to 30 mV. We must take under consideration that the induced voltage is generated during working frequency 1 kHz. If the converter's working frequency will be higher, so the growing and falling time of the current will be smaller and so also the induced voltage will be higher. In due to this fact the motor EMC will be worse. However, the mentioned dependence of induced voltage on frequency is not linear.

Practical automated measuring of magnetic induction B in chosen place A, where the magnetic field magnitude, obtained by simulation, is the worst, did correctness verification of results obtained by simulation. A connection of measuring workplace was realized according Figure 31.

As magnetic induction sensors was utilized the Hall's sensors type A3516 with the sensitivity 2,5 mV/G, Figure 32.

Measured curve of sensor voltage, which is corresponding to magnetic induction B in position A, is displayed in Figure 33., together with the curve of power semiconductor transistor IGBT current i_C, which is connected in DC impulse converter. From the voltage, which is corresponding to the magnetic induction B, was filtered DC component with value 3,7 V by oscilloscope mode enabling to measure only AC component.

Table 3.

i_Z [A]	0	5	8	9,7	11,2	12,4	13,3	14	14,4	14,7	15	10	7	5,3	3,8	2,6	1,7	1	0,6	0,3
t [μs]	0	50	100	150	200	250	300	350	400	450	500	550	600	650	700	750	800	850	900	950

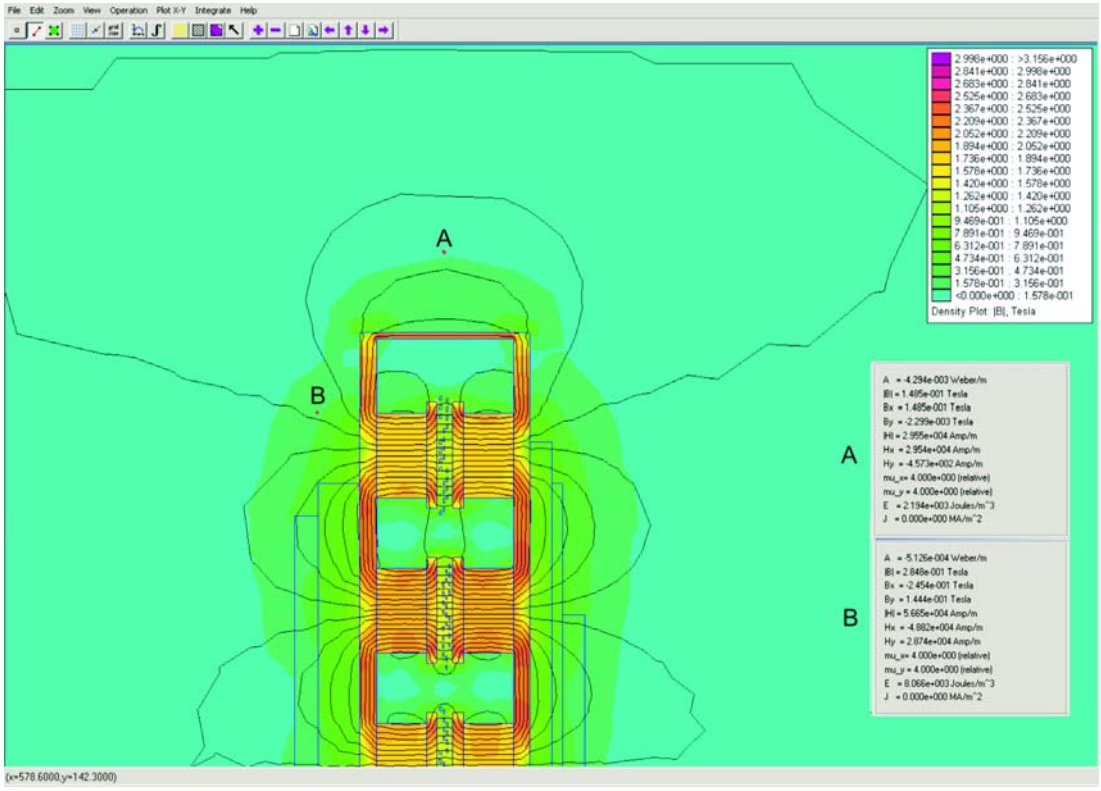

Fig. 25. Magnetic field saturation in surroundings motor space for current value I = 0A

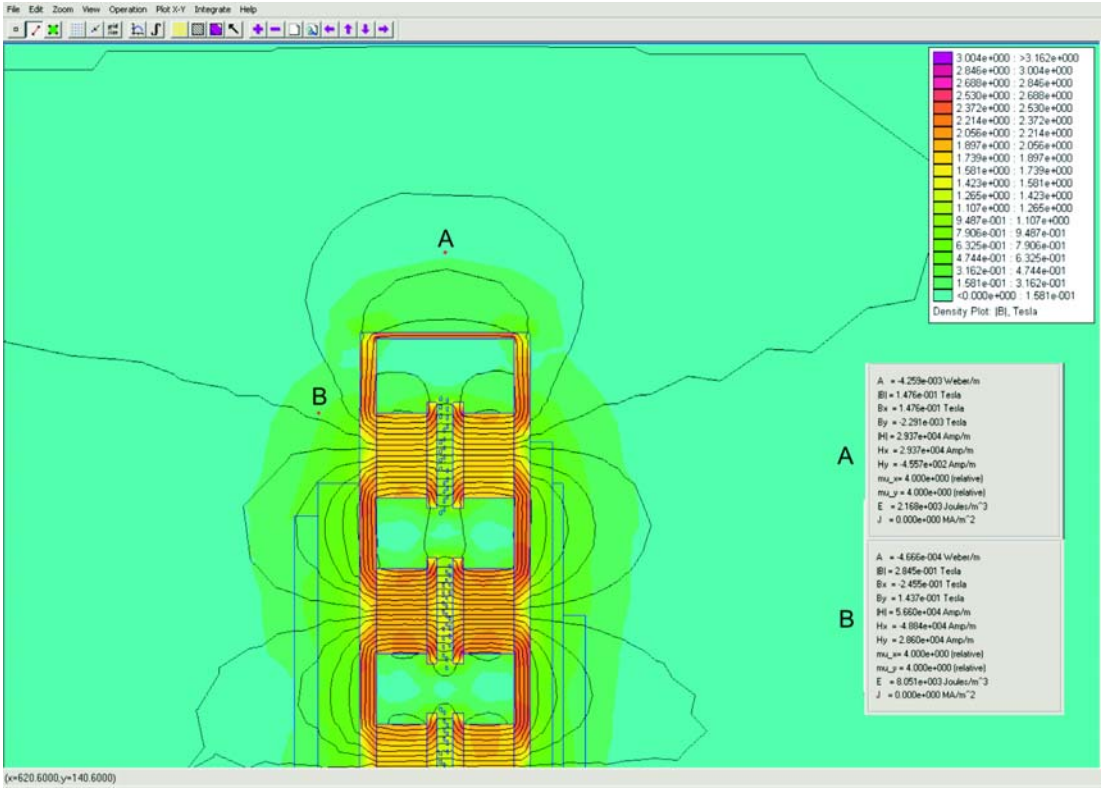

Fig. 26. Magnetic field saturation in surroundings motor space for current value I = 15A

Figure 34 displays the curve of induced voltage sensed by the conductor creating sensing loop with rectangle shape and area S (S = 0,1 x 0,05 m). Figure also shows comparable reference curve of power field effect transistor (IGBT) current i_C.

4.2. Ways for Improving of Motor's EMC

Improving of motor's EMC is possible to understand either as request on absolute value reduction of leakage magnetic field induction B or as request on difference reduction of variable magnetic inductance in given place, which is caused by variable working conditions of electrical machine.

The choice of suitable shielding cover is one way for motor EMC improving. The task of the first cover with relative great magnetic resistance (it should have the smallest relative permeability) is to reduce the magnitude of leakage magnetic field. The task of the second shielding cover with relative small magnetic resistance (it should have the biggest relative

Table 4

t [µs]	i_Z [A]	B_A [T]	B_B [T]	u_{iA} [V]	u_{iB} [V]
0	0	1,485E-01	2,848E-01	0	0
50	5	1,482E-01	2,847E-01	-0,03	-0,01
100	8	1,480E-01	2,846E-01	-0,02	-0,01
150	9,7	1,479E-01	2,846E-01	-0,01	0
200	11,2	1,478E-01	2,846E-01	-0,01	0
250	12,4	1,478E-01	2,845E-01	0	-0,01
300	13,3	1,477E-01	2,845E-01	-0,01	0
350	14	1,477E-01	2,845E-01	0	0
400	14,4	1,477E-01	2,845E-01	0	0
450	14,7	1,476E-01	2,845E-01	-0,01	0
500	15	1,476E-01	2,845E-01	0	0
550	10	1,479E-01	2,846E-01	0,03	0,01
600	7	1,481E-01	2,846E-01	0,02	0
650	5,3	1,482E-01	2,847E-01	0,01	0,01
700	3,8	1,483E-01	2,847E-01	0,01	0
750	2,6	1,484E-01	2,847E-01	0,01	0
800	1,7	1,484E-01	2,847E-01	0	0
850	1	1,485E-01	2,847E-01	0,01	0
900	0,6	1,485E-01	2,848E-01	0	0,01
950	0,3	1,485E-01	2,848E-01	0	0
1000	0	1,485E-01	2,848E-01	0	0

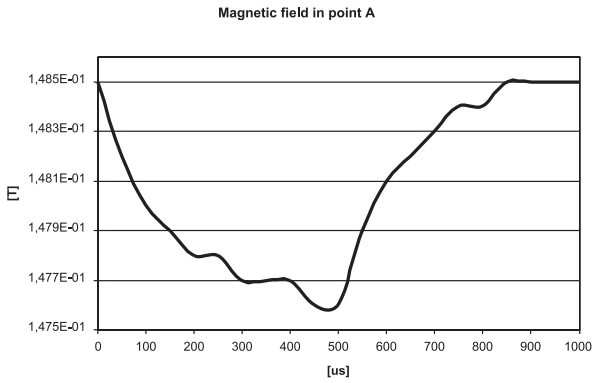

Fig. 27. Magnetic induction B in point A

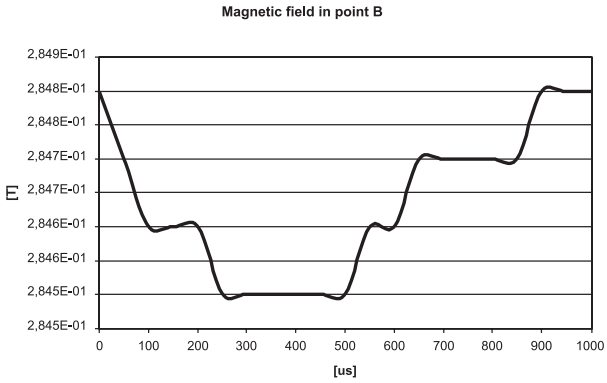

Fig. 28. Magnetic induction B in point B

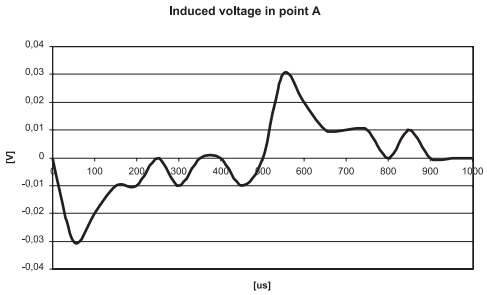

Fig. 29. Induced voltage u_i in point A

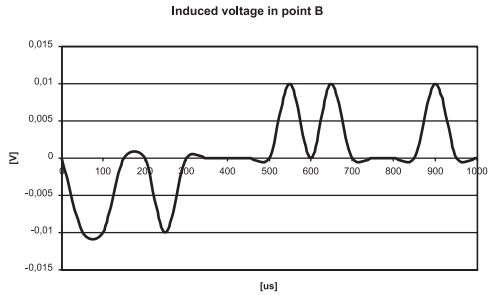

Fig. 30. Induced voltage u_i in point B

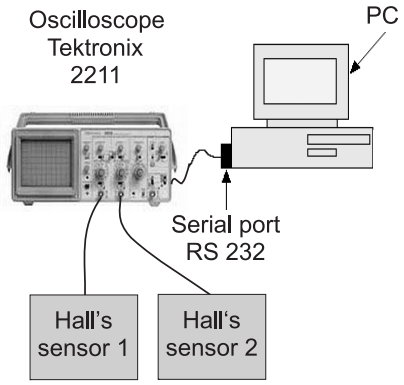

Fig. 31. Automated measuring system controlled by computer

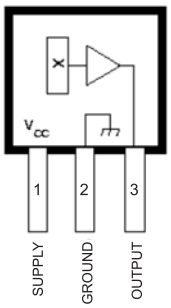

Fig. 32. Linear Hall's sensor of magnetic field type A3516

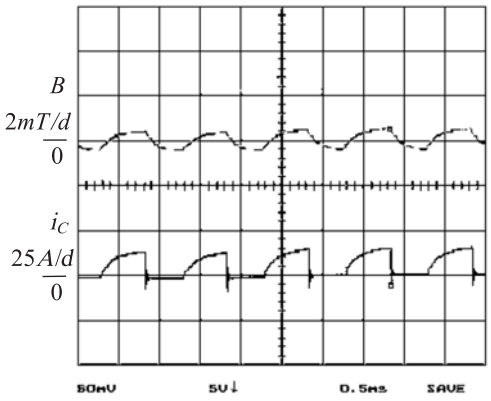

Fig. 33. Measured curves of magnetic induction B and transistor current i_C

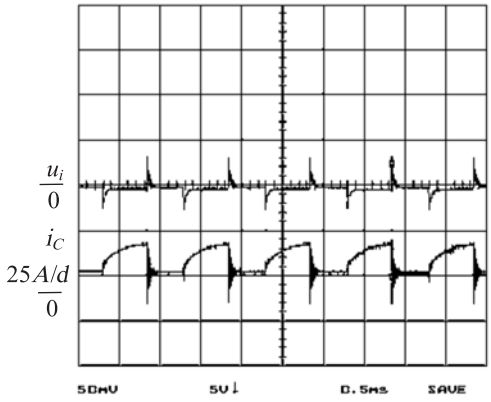

Fig. 34. Measured curves of induced voltage u_i and transistor current i_C

permeability) is vice-versa to create the connection to short for the rest reduced leakage flux.

Designed and recommended construction solution of motor shielding was analyzed by computer simulation. As first shielding cover material was used cooper ($\mu_r = 0{,}9999935$) with thickness 2 mm. The second cover created by supermaloy ($\mu_r = 529095$) had also thickness 2 mm. Simulation was done for motor current values I = 0 A and I = 15 A in due to results comparability with the previous solutions. Obtained results are shown in figures 35 and 36.

By comparing of obtained results with the values in figures 25 and 26 we can find out that the magnetic inductance B value was reduced from value 0,1485 T to new one 0,01211 T under motor current value I = 0 A. It means that one rank down. Magnetic inductance B value was similarly reduced for motor current value I = 15 A from value 0,1476 T to new one 0,01198 T. The change of magnetic inductance, caused by motor current change, was reduced from value $\Delta B = 0{,}0009$ T, in the case of motor without shielding, to new one $\Delta B =$ 0,00013 T, for motor with shielding cover.

The advantage of designed solution consists in its simple realization and possibility of shielding cover reduction in dependence on motor supplying converter's working frequency. If the working frequency will be higher, so the depth of electromagnetic wave penetration d will be smaller

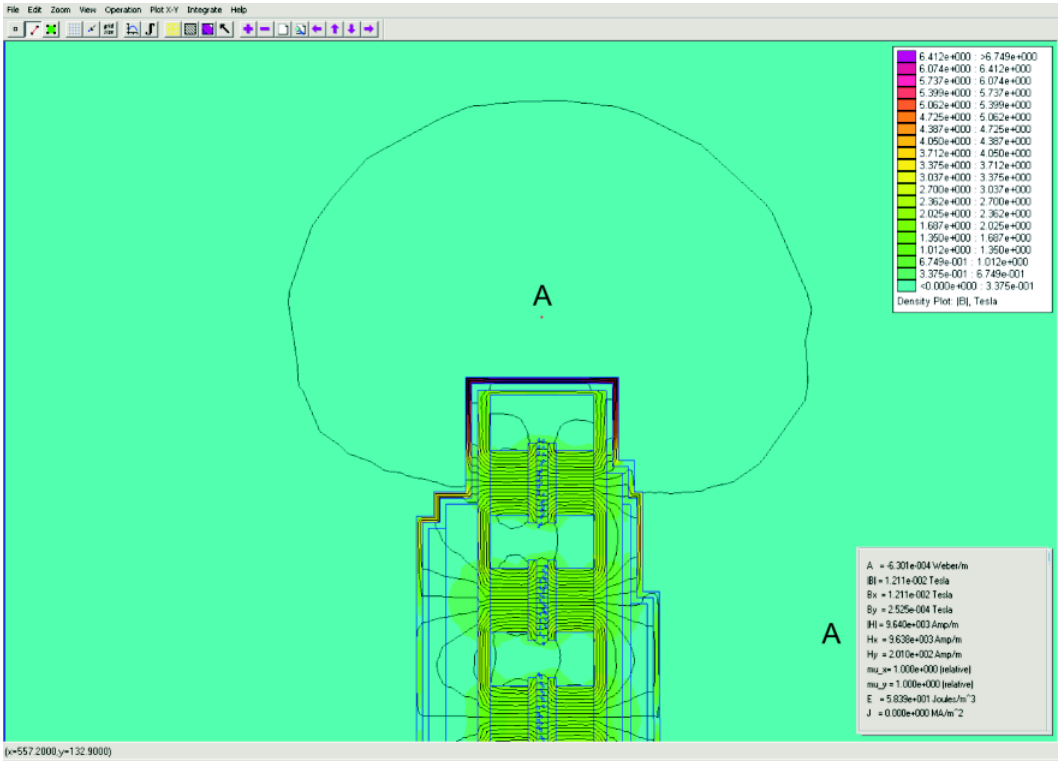

Fig. 35. Magnetic field of shielded DC PM disc motor with the current value 0 A

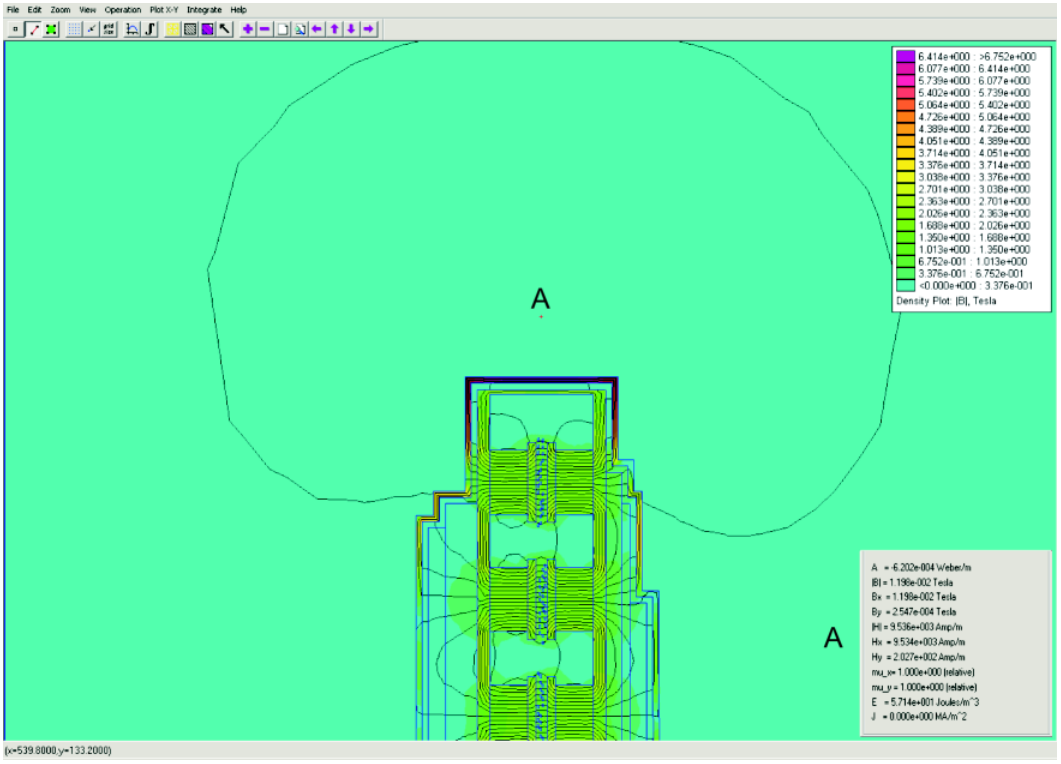

Fig. 36. Magnetic field of shielded DC PM disc motor with the current value 15 A

and so the smaller can be also the thickness of material needed for its damping.

Contrariwise, disadvantage of designed solution consists in the weight, volume and motor price increasing.

The other way, which is fulfilling the requirement for motor's EMC improving, it is increasing of rotor numbers (under the same motor power) so, that the pole pairs of all (in our case three) rotors, which are placed at given stator frame yoke position, has mutually opposite oriented poles. The material with great magnetic resistance (for example cooper) mutually separates individual rotor magnetic circuits. For influence comparing of designed solution is necessary to investigate the arrangement of motor magnetic field with simplified stator frame yoke first. Results obtained by simulation are pictured in Figures 37 and 38.

Results obtained by simulation for motor construction design with three rotors and improved EMC is displayed in Figures 39 and 40.

Fig. 37. Motor magnetic field in the case of motor current value 0 A

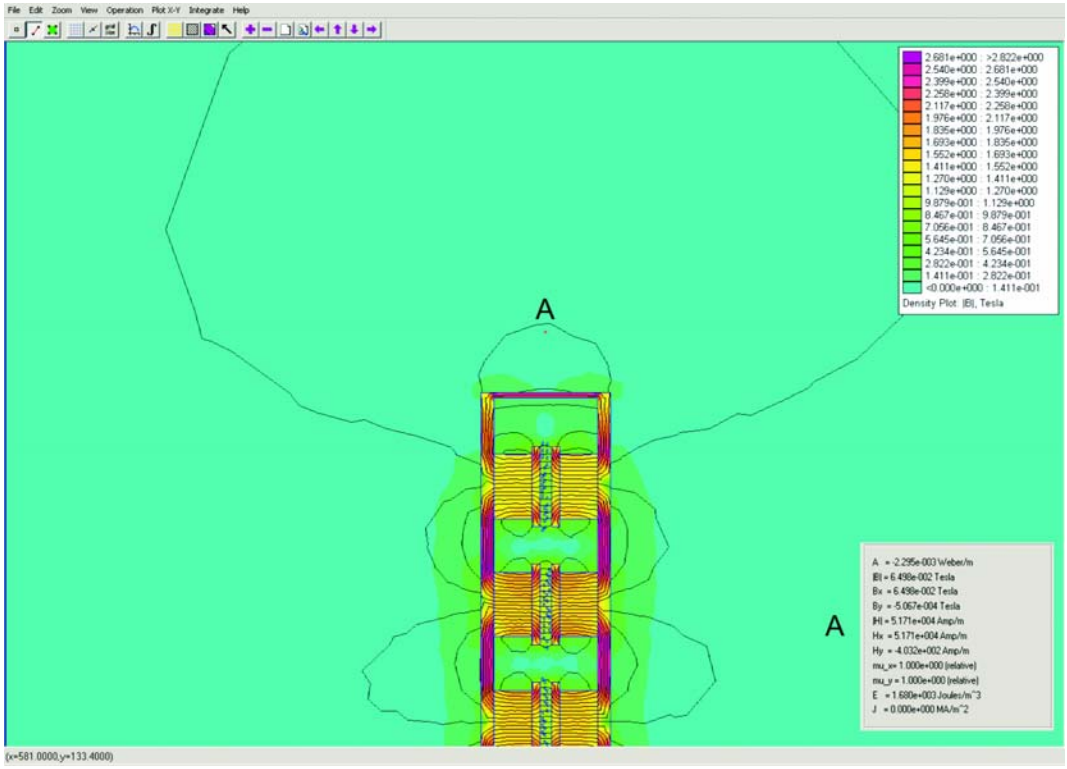

Fig. 38. Motor magnetic field in the case of motor current value 15 A

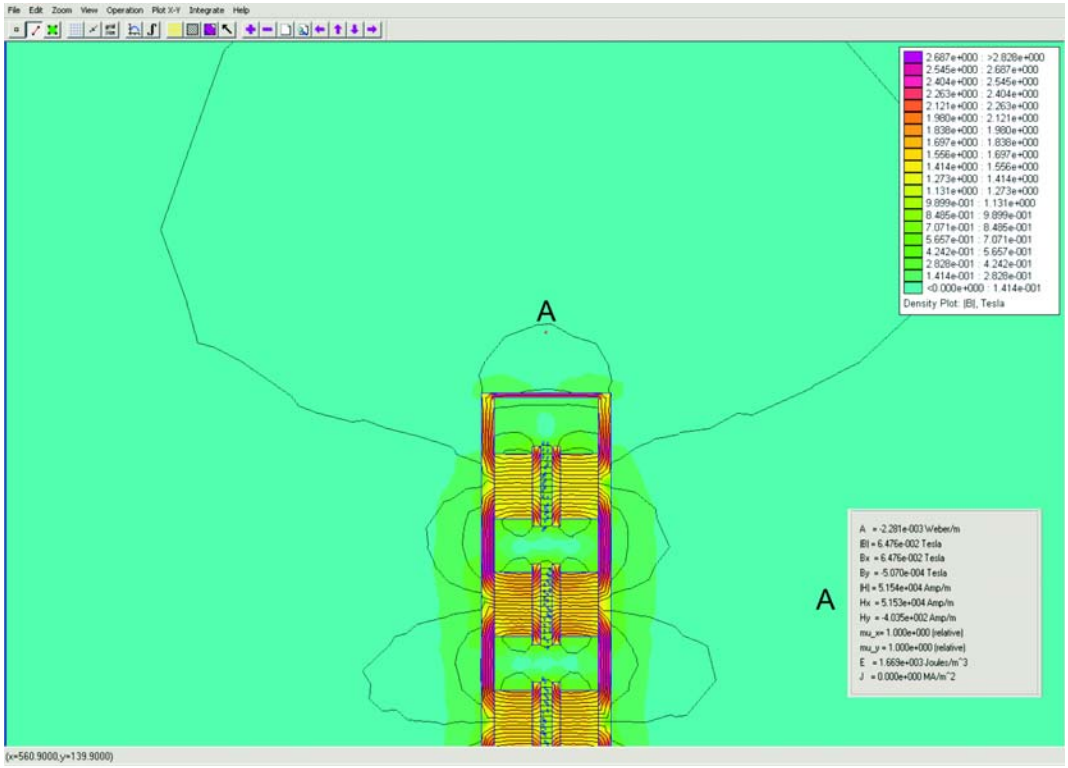

3. CONCLUSION

By obtained values comparing with the values on figures 37 up to 40 we can find out that the magnitude of magnetic inductance *B* was reduced from value 0,06498 T to new one 0,006639 T under motor current I = 0 A. Magnetic inductance *B* value was similarly reduced for motor current value I = 15 A from value 0,06476 T to new one 0,006637 T. The change of magnetic inductance, caused by motor current change, was reduced from value $\Delta B = 0{,}00022$ T to new one $\Delta B = 0{,}000002$ T. Resulting improvement was reached by the fact that for the same motor power the motor with higher number of rotors is required smaller motor current and also by fact that the leakage magnetic fields of individual poles are mutually subtracted and in due to the amount of magnetic field absolute value in surrounding motor space was fallen too. Such constructed motors are advantageous for utilizing at the places, which requires improved EMC parameters.

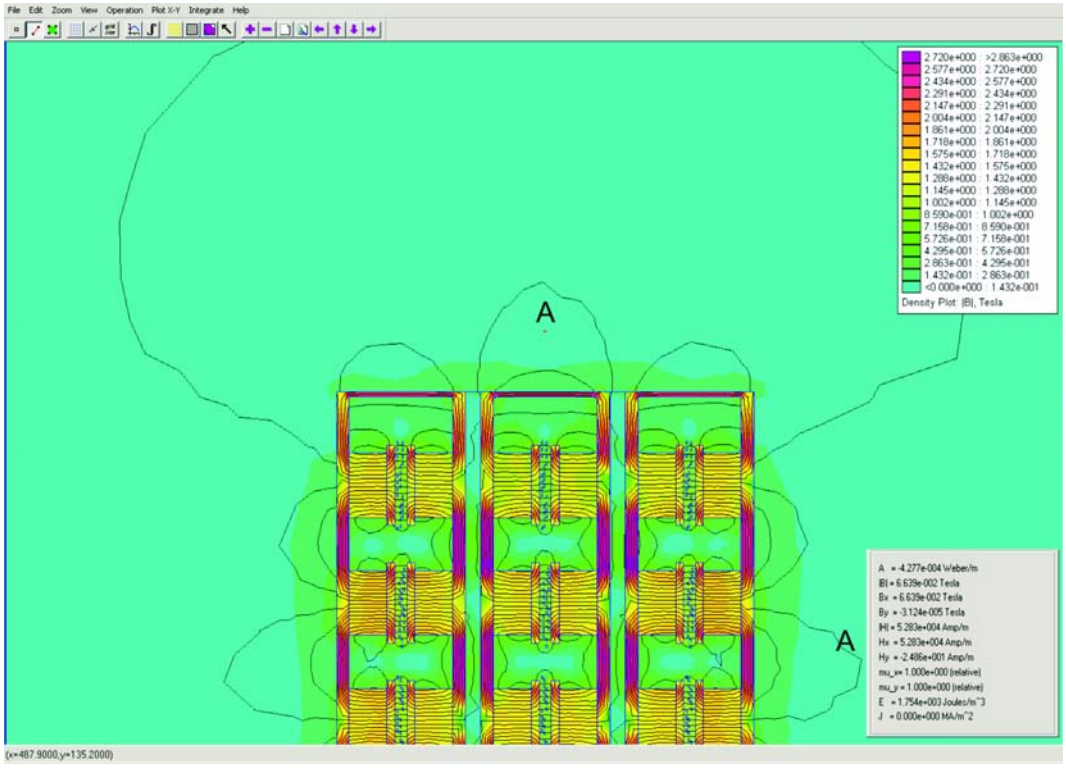

Fig. 39. Magnetic field of motor with three rotors and motor current value 0 A

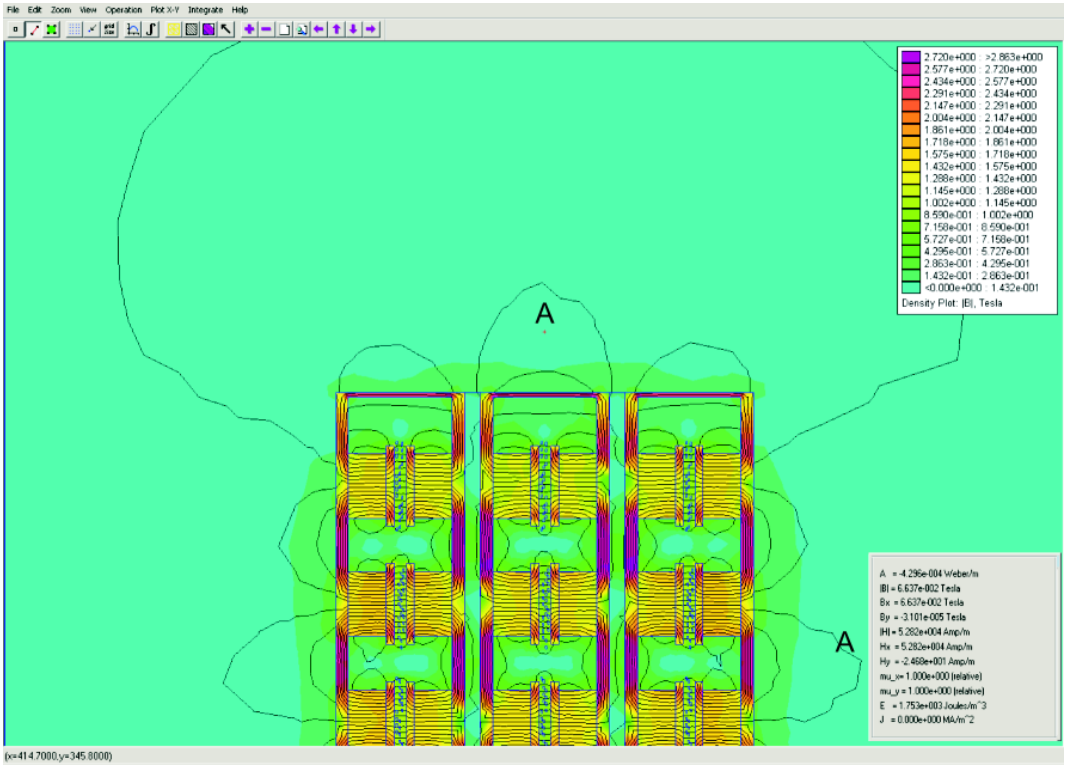

Fig. 40. Magnetic field of motor with three rotors and motor current value 15 A

4. ACKNOWLEDGEMENT

The paper has been prepared under support of Slovak grant project No.1/0376/2003.

REFERENCES

1. Kaňuch J.: *Electromagnetic compatibility of power semiconductor converters.* Dissertation thesis, FEI TU Košice, 2005.
2. Kotal M., Novotný P., Voženílek P.: *Calculation examples of rotation electrical machines, Editorial centre of* ČVUT in Prague, 1988.
3. Kováč D., Kováčová, I.: *Infuence of Utilizing Static Power Semiconductor Convertors on Quality of Electrical Power Line Parameters,* Quality Innovation Prosperity, 2001, No.1, pp.74–84.

4. Kováč D., Kováčová I.: *Power transistors MOSFET and IGBT.* Elfa s.r.o. Publisher, Košice, 1996, 117 pages, ISBN 80-88786-34–7.
5. Kováč, D., Kováčová I., Šimko V.: Analysis of electric circuits I. Košice, Akris Publisher, 2001, 112 pages, ISBN 80-968666-1-3.
6. Kováč, K., Lenková, A.: *Electromagnetic compatibility (working letters).* Methodical centre, Bratislava 1999.
7. Kováčová I.: *EMC of Power DC Electrical Drives*, Journal of Electrical Engineering, Vol. 5, 2005, No.1, pp. 61–66.
8. Kováčová I., Kováč D.: *EMC Compatibility of Power Semiconductor Converters and Inverters*, Acta Electrotechnica et Informatica, Vol.3, 2003, No.2, pp.12–14.
9. Mayer D., Ulrych B., Škopek M.: *Solving of the electromagnetic fields by the modern software products.* EE Journal, Vol. 7, 2001, No.1.
10. Pálka R.: *Electrical machines IV — designing of the DC machines.* Editorial centre of SVŠT in Bratislava, 1983.
11. *Servalco Servomotor*, catalogue of Axem company.
12. Vaculíková P., Vaculík P. a kol.: *Elektromagnetic compatibility of electrical engineering systems,* GRADA Publishing, 1998.

Irena Kováčová (Assoc. Prof., eng., CSc.)
Born in 1958. She finished her studies in 1982 at the Technical University of Košice, Department of Electrical Drives, direction - Power electronics with excellent evaluation. From this time she has worked at the Department of Electrical Drives, first as assistant lecturer and now as associate professor. In 1988 she has got her doctoral diploma. In 1991 she has got the Award of Minister of Education for Development of Science and Technology. Her working interest is mainly focused to the field of power electronics, especially to the construction of converters and inverters with new perspective elements and computer simulation of new power semiconductor parts and devices.
Address:
Department of Electrical Drives and Mechatronics,
Technical University of Košice,
Letná 9, 042 00 Košice, Slovak Republic,
E-mail: Irena.Kovacova@tuke.sk

Ján Kaňuch (eng.)
Born in 1963. He finished his studies in 1986 at the Technical University of Košice, Department of Electrical Drives and direction - Electrical machines. From this time he has worked at the Department of Electrical Drives as assistant lecturer. His working interest is mainly focused to the field of construction of electrical machines, electrical equipments for motor-cars and electrical apparatuses.
Address:
Department of Electrical Drives and Mechatronics,
Technical University of Košice,
Letná 9, 042 00 Košice, Slovak Republic,
E-mail: Jan.Kanuch@tuke.sk

Dobroslav Kováč (Prof., eng., CSc.)
Born in 1961. He finished his studies in 1985 at the Technical University of Košice, Department of Electrical Drives, direction – Power electronics with excellent evaluation. Then he worked as research worker at the Department of Electrical Drives. His research work was focused to the practical application of new power semiconductor devices. In 1989 he has got the Award of Minister of Education for Development of Science and Technology. From 1991 he has worked as assistant lecturer at the Department of Theoretical electrical engineering and Electrical measurement. He got his doctoral diploma in 1992 for the work on the field of power electronics. From 2000 he worked as professor and his working interest is now focused mainly to the field of computer simulation of power electronic circuits and automated computer measuring. From 1999 he is also working as Vice-dean of faculty.
Address:
Department of Theoretical Electrical Engineering and Electrical Measurement,
Park Komenského 3, 042 00 Košice, Slovak Republic,
phone: (+421) 602 2516, (+421) 602 20 24,
E-mail: Dobroslav.Kovac@tuke.sk